13th International Symposium on Turbulence and Shear Flow Phenomena (TSFP13)
Montreal, Canada, June 25–28, 2024

WHY HYDROGEN-AIR PREMIXED FLAMES PROPAGATE FAST(ER) IN TURBULENCE?

Yuvraj[1], **Swetaprovo Chaudhuri**[1]
[1]University of Toronto Institute for Aerospace Studies
University of Toronto, Toronto, Canada
email: y.yuvraj@mail.utoronto.ca

ABSTRACT

Intrinsically fast hydrogen-air premixed flames can be rendered much faster in turbulence. Understanding how turbulence affects the displacement speeds S_d in lean hydrogen-air flames is crucial for systematically developing hydrogen-based gas turbines and spark ignition engines. This paper presents fundamental insights into the variation of S_d by investigating how the disrupted flame structure affects S_d and vice-versa. To that end, we investigate three DNS cases of lean hydrogen-air mixtures with effective Lewis numbers (Le) ranging from about 0.5 to 1, over Karlovitz number (Ka) range of 100 to 1000. Suitable comparisons are made with the closest canonical laminar flame configurations at identical mixture conditions, elucidating their suitability and limitations in expounding turbulent flame properties. We focus on the statistical variation of S_d and the changes in flame structure at near-zero curvature surface locations, which are most probable and represent the average flame structure in large Ka flames. We find that lean hydrogen flames, on average, could be thinned or thickened with respect to their standard laminar counterpart but always thickened compared to the corresponding strained laminar flames at equal average tangential strain-rate conditions. While turbulent straining enhances the S_d in most parts of the highly lean premixed flames through Le effects, on average, the enhancement is different from those achieved in strained laminar flames due to local flame thickening. This thickening is primarily due to reversal in the direction of the S_d underpinned by ubiquitous, non-local, cylindrical flame-flame interaction events occurring within the flame structure in these large Ka flames.

Introduction

Hydrogen is considered a promising alternative fuel to achieve sustainable energy solutions for both transportation and stationary applications. Ultra-lean premixed combustion of hydrogen has the potential of achieving high efficiency and low NO_x emissions (Gkantonas *et al.* (2023)), but some critical challenges need to be overcome before its full implementation in practical engineering systems. One notable issue is the extremely high flame speed that often occurs erratically in the presence of strong turbulence, leading to flashbacks and damage to the injector system. A similar situation is encountered for SI engines where high flame speed and reactivity of stratified hydrogen-air mixtures may result in pre-ignition.

These issues have revived research interests in the diffusive-thermal instability theory (Zeldovich (2014)) relevant to lean hydrogen-air premixed flames. Recent computational studies have further explored its implications in the context of high Reynolds number conditions for atmospheric and high-pressure hydrogen flames (Song *et al.* (2021, 2022); Chu *et al.* (2023); Rieth *et al.* (2022, 2023); Howarth *et al.* (2023); Lee *et al.* (2023)), in which the local flame zones are subjected to significantly higher strain and curvatures. The overarching findings of these recent studies suggest that the diffusive-thermal instability of ultra-lean hydrogen may lead to significantly increased burning rates by the preferential diffusion of hydrogen into the reaction zones.

The present study attempts to explain the flame speed enhancement of lean hydrogen-air turbulent flames by combining Le effects in tangentially strained flames with flame thickening caused by non-local flame-flame interaction in instability-free conditions. Earlier studies on local flame displacement speeds investigated the effect of local curvature and strain (Echekki & Chen (1996); Peters *et al.* (1998)) and Lewis number (Chakraborty & Cant (2005)) in turbulent flame context. More recently, a Lagrangian analysis of flame particles (Chaudhuri (2015)) from their genesis to annihilation (Dave *et al.* (2018)) showed that for moderate Ka, near-unity Le flames, flame-flame interaction leading to annihilation at large negative local curvatures κ results in very large excursions of the density-weighted flame displacement speed $\widetilde{S_d}$ over its unstretched, standard laminar value S_L.

A theoretical analysis of the interacting preheat zones of cylindrical, laminar, premixed, inwardly propagating flame (IPF) extended and quantified (Dave & Chaudhuri (2020)) the curvature-based scaling (Peters (2000)). At very large Ka, the flame-flame interaction becomes highly frequent and localized at the iso-surface level (Yuvraj *et al.* (2023)), but the curvature-based scaling was found to remain valid statistically (Yuvraj *et al.* (2022)). The surprising finding that a simple 1D laminar flame model could successfully describe the statistically averaged $\widetilde{S_d}$ characteristics at large negative κ in turbulence may be explained by the considering that: 1) flame-flame interaction is a fast event during which the local turbulence remains frozen, 2) at large κ, local flame structures are near or sub-Kolmogorov length scales, and 3) turbulence folds the propagating flame surfaces into a locally cylindrical form (Pope *et al.* (1989); Yuvraj *et al.* (2023)). These findings suggested that, while the flame-flame interaction may exhibit many complex topologies (Griffiths *et al.* (2015); Brouzet *et al.* (2019); Trivedi *et al.* (2019)), an IPF configuration can serve as a canonical model to describe the statistical behavior of $\langle \widetilde{S_d} | \kappa \rangle$ at large negative curvature for near-unity Le cases.

In this study, we extend the IPF analysis to characterize the $\widetilde{S_d}$ behavior of very large $Ka \sim \mathcal{O}(100-1000)$ lean hydrogen-air premixed flames, for which the *Le* is in the range of 0.5 - 1.0. It is hypothesized that the present configurations are nearly free of the intrinsic diffusive-thermal instability effect due to very large *Ka* (Chaudhuri *et al.* (2011); Chomiak & Lipatnikov (2023)), yet such a configuration may provide insights into the observed anomaly of large flame speed enhancement of the turbulent, lean hydrogen-air flames. The main research questions of the study are: (a) Can the large negative κ behavior of ultra-lean hydrogen-air premixed turbulent flames be described by the laminar cylindrical flame model? (b) To what extent is $\langle \widetilde{S_d} \rangle$ enhanced beyond S_L for non-unity *Le* hydrogen-air premixed flames at $Ka \approx 100$? (c) What is the flame thickening mechanism in intense turbulence, and its implications on the $\langle \widetilde{S_d} \rangle$? These questions are addressed by analyzing three direct numerical simulation (DNS) datasets at different *Le* (Matalon *et al.* (2003)) and *Ka*.

Methodology

Table 1. Non-dimensional parameters for the DNS datasets.

Case	Re_t	Ka	ϕ	Le_{eff}
Le05Ka100	799.6	115.4	0.4	0.48
Le08Ka1000	699.5	1125.7	0.7	0.76
Le1Ka100	996.2	100.1	0.81	0.93

Table 1 presents the details of the DNS cases comprising of statistically planar, lean H_2-air turbulent premixed flame at atmospheric pressure. Le05Ka100 and Le1Ka100 are computed using an open-source reacting flow DNS solver called the Pencil Code (Brandenburg *et al.* (2018)). Le08Ka1000 was previously generated and investigated (Song *et al.* (2021); Yuvraj *et al.* (2022, 2023)) (named as F2) but included here for additional insights. For the present scope of work, the leanest case Le05Ka100 is of particular interest. A detailed chemical mechanism with 9 species and 21 reactions by Li *et al.* (2004) was used to model the H_2-air chemistry. The DNS is performed by superimposing homogeneous isotropic turbulence generated in a cube on the mean flow and fed through the inlet of a cuboidal domain to interact with an initial planar laminar flame. The Navier-Stokes characteristic boundary conditions (NSCBC) were imposed in the inflow and outflow direction, with periodic boundary conditions in the transverse directions. As for the model analysis, one-dimensional simulations for cylindrical, laminar, premixed, inwardly propagating flames (IPF) and symmetric, laminar, premixed, counter flow flames (CFF) (Law (2006)) with reactant mixtures entering from both inlets at varying inlet velocities for the latter, were also performed using the Pencil Code and Chemkin, respectively, after ensuring that both solvers produce solutions identical to the standard laminar case.

Results

The local displacement speed, S_d is evaluated from the DNS data from the right-hand side of the energy equation:

$$S_d = \frac{1}{\rho C_p}\left[\frac{\nabla\cdot(\lambda'\nabla T)}{|\nabla T|} - \frac{\rho\nabla T\cdot\sum_k(C_{p,k}V_kY_k)}{|\nabla T|} - \frac{\sum_k h_k\dot{\omega}_k}{|\nabla T|}\right] \quad (1)$$

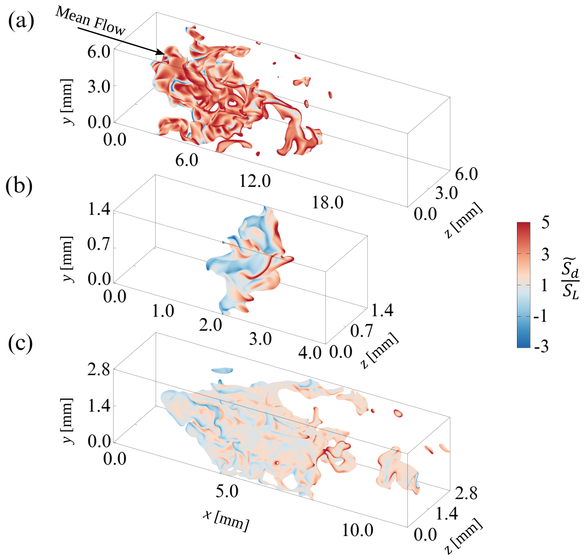

Figure 1. Flame surface ($c_0 = 0.2$) for (a) Le05Ka100 (b) Le08Ka1000 (c) Le1Ka100 colored by $\widetilde{S_d}/S_L$.

where λ', V_k, h_k and $\dot{\omega}_k$ are the thermal conductivity of the mixture, the molecular diffusion velocity, enthalpy, and net production rate of the kth species at a given isotherm, respectively. $C_{p,k}$ and C_p are the constant-pressure specific heat for the kth species and for the bulk mixture, respectively.

Here we use a progress variable c defined as a function of temperature as $c = (T - T_u)/(T_b^\circ - T_u)$, where T_b° is the adiabatic flame temperature. While the actual burned gas temperature of the lean flames may be different from T_b°, considering that the temperature on an iso-mass fraction surface may change even more and that the flame speed depends most strongly on temperature (Law (2006)), temperature-based c is adopted as in Chaudhuri *et al.* (2017). It has been ascertained that results with the progress variable based on hydrogen mass fraction, $c_Y = 1 - Y_{H_2}/Y_{H_2,u}$, are qualitatively similar to all the results presented in this paper. Recognizing the caveats presented in (Howarth & Aspden (2022)) due to super-adiabatic temperatures, the analysis is restricted to $c \leq 0.8$.

Figure 1 presents the iso-surface $c = c_0$ where $c_0 = 0.2$ colored with normalized density weighted flame displacement speed, $\rho S_d/\rho_u S_L = \widetilde{S_d}/S_L$ at a given time instant. $\widetilde{S_d}/S_L$ attains a value up to five at the large negatively curved trailing edge of the flame surfaces for all cases due to flame-flame interaction. Le05Ka100 shows $\widetilde{S_d}/S_L > 1$ for most parts of the iso-scalar surface, in contrast to Le08Ka1000 and Le1Ka100, for which most of the regions on the flame surface have $\widetilde{S_d} \approx S_L$. The widespread enhancement of average $\widetilde{S_d}$ for Le05Ka100 is also evident from Fig. 2, which presents the joint probability density function (JPDF) of $\widetilde{S_d}/S_L$ versus the non-dimensional curvature, $\kappa\delta_L$ for Le05Ka100 at $c_0 = 0.05$, 0.2, 0.4 and 0.6. The blue line shows its normalized conditional mean for a given κ, $\langle \widetilde{S_d}|\kappa\rangle/S_L$. The vertical dotted red lines indicate $\langle\kappa\delta_L\rangle \approx 0$ for all c_0. The IPF simulation results are overlaid in solid black lines with black circular symbols, and the corresponding analytical model: $\widetilde{S_d} = -2\widetilde{\alpha}_0\kappa$ in dashed black line. The two overarching observations are the following: 1) The blue curve $\langle \widetilde{S_d}|\kappa\rangle/S_L$ asymptotically matches the IPF simulation as well as the analytical model prediction for $\kappa\delta_L \ll -1$ for all c_0. The slope of $\langle \widetilde{S_d}|\kappa\rangle$ of the asymptotic limit increases with c_0, consistent with the IPF and model prediction. 2) The horizontal solid red line and the red arrow indicate the net enhancement of $\widetilde{S_{d,0}} = \langle \widetilde{S_d}|_{\kappa=0}\rangle$ by several factors over S_L. This observation

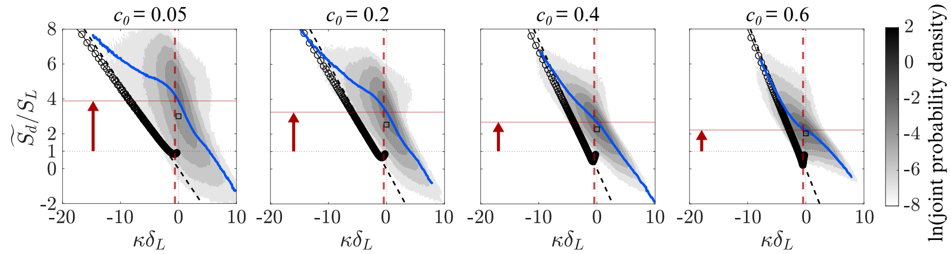

Figure 2. Joint probability density function (JPDF) of normalized density-weighted flame displacement speed, $\widetilde{S_d}/S_L$, and normalized curvature,$\kappa\delta_L$, for iso-scalar, $c_0 = 0.05, 0.2, 0.4$ and 0.6 for Le05Ka100. The grey scale represents the natural logarithm of the JPDF magnitude. The solid blue curve is the conditional mean, $\langle\widetilde{S_d}|\kappa\rangle/S_L$, at a given κ, obtained from the DNS. The solid horizontal and the dashed vertical red lines show $\widetilde{S_{d,0}}/S_L$ and $\langle\kappa\delta_L\rangle$, respectively. The mean $\langle\rangle$ of the variables conditioned on $\kappa = 0$ is calculated over a narrow range $-0.05 < \kappa\delta_L < 0.05$. The dashed black line represents the analytical model, $\widetilde{S_d} = -2\widetilde{\alpha}_0\kappa$ and the solid black curve with circular markers represent the IPF results. The hollow square symbol marks $\widetilde{S_{d,0}}$ conditioned on zero tangential strain rate, $\widetilde{S_{d,0}}|_{a_T=0}$.

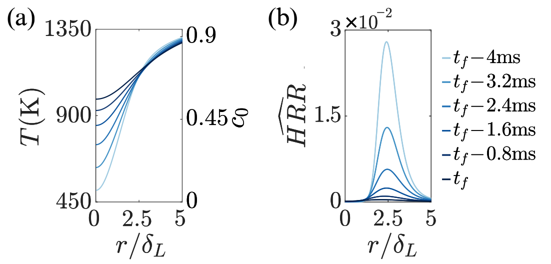

Figure 3. Radial temperature and normalized heat release rate profiles obtained from IPF for conditions as that of Le05Ka100 at various time instances during flame-flame interaction.

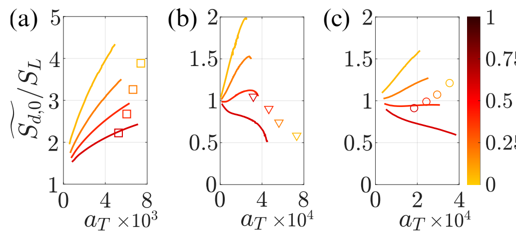

Figure 4. The variation of $\widetilde{S_{d,0}}/S_L$ with $\langle a_{T,DNS}\rangle$ for (a) Le05Ka100 (b) Le08Ka1000 (c) Le1Ka100 in hollow markers. The solid lines represent CFF solutions. The colorscale corresponds to c_0.

is in contrast with higher $Le \approx 0.7-1.0$ cases (Dave & Chaudhuri (2020); Yuvraj *et al.* (2022); Chaudhuri & Savard (2023); Yuvraj *et al.* (2023)), where $\widetilde{S_{d,0}} \approx S_L$ at most c_0 (Yuvraj *et al.* (2023)), but similar to the observation in Chu *et al.* (2023). First, we elaborate on observation 1, followed by a detailed investigation of observation 2 in the rest of the paper.

Figure 3 shows the temporal evolution of temperature and the heat release rate (HRR) profiles obtained from the IPF simulation at the thermodynamic conditions of Le05Ka100 during the annihilation event. HRR is normalized by its maximum standard laminar value. Note that the HRR profiles barely exist with 3% of the laminar value even before the onset of interaction due to strong negative stretch rates and Le effects satisfying the inherent assumption of non-interacting heat release layers in the interaction model (Dave & Chaudhuri (2020); Yuvraj *et al.* (2023)) describing the $\widetilde{S_d}$ at large negative κ resulting in the agreement of the DNS results with the theory.

Given that a 1D cylindrical flame model successfully explained the behavior of $\widetilde{S_d}$ at large negative κ in turbulence, the large increase in $\widetilde{S_{d,0}}/S_L$ at $\kappa\delta_L \approx 0$ implies that this behavior may be explained by the tangential strain rate a_T and Le effect. This will be attempted by the 1D premixed counterflow flame (CFF) (Coulon *et al.* (2023); Detomaso *et al.* (2023); Lee *et al.* (2022)), with the a_T representing the mean value for the DNS data. Figure 4 presents the variation of $\widetilde{S_{d,0}}/S_L$ with a_T from the CFF simulations at different values of c_0 (denoted in color scale). The data from the DNS simulations for the mean tangential strain rate ($\langle a_{T,DNS}\rangle$) at $c_0 = 0.05, 0.2, 0.4$ and 0.6 are shown in open symbols. Comparing results from CFF simulations at $a_T = \langle a_{T,DNS}\rangle$, it is found that $\widetilde{S_{d,0}}/S_L > 1$ under positive straining for Le05Ka100 and Le1Ka100 for c_0 before peak heat release. The CFF trends agree with Vance *et al.* (2021). However, CFF provides no solution at high $a_T(c_0 = 0.5, 0.2$ for Le05Ka100, $c_0 = 0.05, 0.2$ for Le1Ka100) and even if the solution exists, it is larger (smaller) compared to $\widetilde{S_{d,0}}$ for c_0 before (after) peak heat release rate. Overall, even though the trends of CFF solutions and $\widetilde{S_{d,0}}$ (Le05Ka100 andLe1Ka100) are similar with increasing a_T, they are quantitatively different. Moreover, for Le08Ka1000 the trends in $\widetilde{S_{d,0}}$ are very different from those of CFF. Thus, CFF falls short in capturing the complete behavior of $\widetilde{S_{d,0}}$ and the corresponding average structure at $\kappa = 0$. This could be due to history or transient effects in turbulent flames (Im *et al.* (1996)), as such, conditioning on $a_T = 0$ also yields $\widetilde{S_{d,0}}|_{a_T=0} > S_L$ (black squares in Fig. 2) (Chu *et al.* (2023)). Hence, it is imperative to connect $\widetilde{S_{d,0}}$ with the local flame structure. It is first recognized that the magnitude of the normalized gradient ratio of the progress variable, $|\nabla c|_{c_0}/|\nabla c|_{c_0,L}$ is a possible measure of the local flame structure compared to its standard laminar counterpart. Thus, we correlate $\widetilde{S_{d,0}}/S_L$ and the normalized mean absolute gradient of the progress variable conditioned on $\kappa = 0$, $\langle|\widehat{\nabla c}|_{c_0}|_{\kappa=0}\rangle$ based on Eq. 2.

$$\frac{\widetilde{S_d}|_{\kappa=0}}{S_{L_{c,0}}} \approx \frac{|\nabla c|_{c_0}|_{\kappa=0}}{|\nabla c|_{c_0,L}} = |\widehat{\nabla c}|_{c_0}|_{\kappa=0} \quad (2)$$

Figure 5 shows the results for the three DNS cases under study as well as cases F1, F4, P3 and P7 from previous studies (Song *et al.* (2021); Yuvraj *et al.* (2022, 2023)) for a wider range of Ka and Le conditions. The results from CFF simulations at all a_T are shown in different line types, whereas the solid markers correspond to CFF solutions at $a_T = \langle a_{T,DNS}\rangle$ conditioned on the same isotherms. The dash-dotted grey line denotes Eq. 2. Figure 5a includes the results (DNS and CFF) for c_0 before the maximum heat release rate and Fig. 5b at all c_0 values.

Overall, $\widetilde{S_{d,0}}/S_L$ show a good correlation with $\langle|\widehat{\nabla c}|_{c_0}|_{\kappa=0}\rangle$ for all DNS cases and CFF solutions in the preheat zone. This observation is consistent with that in Yuvraj *et al.* (2023) but generalizes the findings to a much wider range of Le conditions. Figure 5c shows that $\langle\widetilde{S_d}\rangle/S_L$

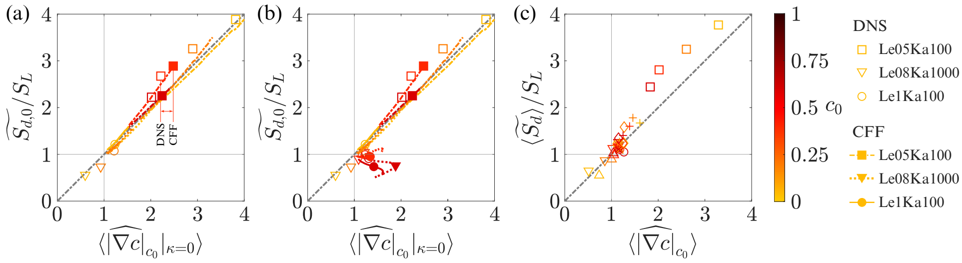

Figure 5. Correlation of $\widetilde{S_{d,0}}/S_L$ with $\langle|\widehat{\nabla c}|_{c_0}|_{\kappa=0}\rangle$ for DNS and laminar CFF (a) in the preheat zone (c_0 before maximum heat release rate only) (b) over the entire flame structure at $c_0 = 0.05, 0.2, 0.4$ and 0.6. Hollow symbols represent DNS data, and filled symbols of the same shape represent CFF data at the same thermodynamic conditions, with $a_T = \langle a_{T,DNS}\rangle$. Lines show CFF solutions over varying a_T. (c) Correlation of $\langle\widetilde{S_d}\rangle/S_L$ with $\langle|\widehat{\nabla c}|_{c_0}|\rangle$ for the present cases and those from previous studies Song *et al.* (2021); Yuvraj *et al.* (2022, 2023). Data from these additional cases are denoted by: F1: '☆', F3: '×', F4: '△', P3: '◊', P7: '+'.

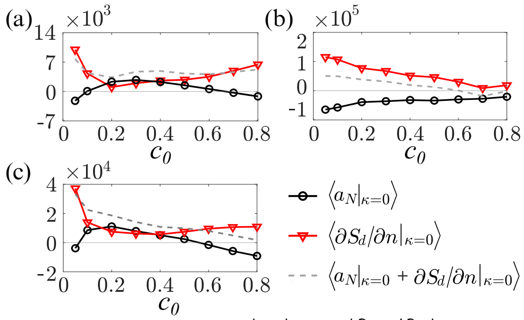

Figure 6. The variation of $\langle a_N\rangle$ and $\langle\partial S_d/\partial n\rangle$ conditioned on $\kappa = 0$ for (a) Le05Ka100 (b) Le08Ka1000 (c) Le1Ka100 in hollow markers. The dashed grey curve denotes their sum.

and $\langle|\widehat{\nabla c}|_{c_0}\rangle$ are also very well correlated since for all the surfaces $\langle\kappa\delta_L\rangle \approx 0$. Nevertheless, from the data it is apparent that Le05Ka100 case exhibits more thinned preheat zones with increased $\langle|\widehat{\nabla c}|_{c_0}|_{\kappa=0}\rangle$, resulting in large $\widetilde{S_{d,0}}/S_L$, while Le08Ka1000 and Le1Ka100 cases show local broadening in preheat zone thickness with $\widetilde{S_{d,0}}/S_L < 1$. While the suggested correlations show overall good agreement for all *Le* conditions under study, an additional important issue must be discussed. For the Le05Ka100 case, the data points from CFF calculations at $a_T = \langle a_{T,DNS}\rangle$ (shown in filled symbols) appear at higher values along both axes when compared to the DNS (shown in hollow symbols but of the same shape), in Fig. 5(a). This implies that the turbulent flame segment subjected to the same average a_T has a relatively smaller net flame thinning effect than the steady laminar flame counterpart, suggesting some degree of attenuation in the effect of straining in the turbulent flame. The same effect is revealed in Le08Ka1000 and Le1Ka100 cases, where the effect of turbulence results in a net broadening of the flame thickness. Therefore, there appears to be a consistent effect residing in turbulence-flame interaction where the turbulent flames are broadened on average compared to equivalent laminar strained flames.

For further insights, we consider the transport equation for $|\widehat{\nabla c}|$ in the Lagrangian form at the flame surface (Dopazo *et al.* (2015); Chaudhuri *et al.* (2017); Wang *et al.* (2017)):

$$\frac{\widetilde{D}|\widehat{\nabla c}|}{\widetilde{D}t} = -\left[a_N + \frac{\partial S_d}{\partial n}\right]|\widehat{\nabla c}| \tag{3}$$

where a_N is the fluid motion-induced normal strain rate and $\partial S_d/\partial n$ is the normal strain rate due to flame propagation with $n = -\nabla c/|\nabla c|$ being the local normal in the direction of the reactants. Each term on the right-hand side shows the mechanism of thickening or thinning of the flame structure. In steady flames, the sum is identically zero. Fig. 6 shows the variation of the mean a_N and $\partial S_d/\partial n$ conditioned on $\kappa = 0$ with c_0 for all the cases. Dopazo *et al.* (2015) reported $\langle a_N\rangle > 0$ and $\langle\partial S_d/\partial n\rangle < 0$ for low *Ka* flames. In the present study, we found that for all *Ka* and *Le*, $\langle\partial S_d/\partial n|_{\kappa=0}\rangle > 0$, similar to those observed in large *Ka* methane-air Bunsen flames Wang *et al.* (2017) but in direct contrast to planar laminar unstrained/strained flame behavior where $\partial S_d/\partial n = -a_N < 0$. For $Ka \sim 100$ cases, $\langle a_N|_{\kappa=0}\rangle > 0$ possibly due to dilatation, while for $Ka \sim 1000$, $a_N < 0$. The nature of $\langle a_N|_{\kappa=0}\rangle$ in turbulent premixed flame based on the alignment of the smallest principal strain rate and the normal to the iso-scalar surfaces have been discussed (Chakraborty & Swaminathan (2007); Chaudhuri *et al.* (2017)). Unlike a steady laminar flame, where positive a_N and negative $\partial S_d/\partial n$ balance out, in these turbulent flames, the net contribution remains positive (dashed curve) primarily due to $\langle\partial S_d/\partial n|_{\kappa=0}\rangle > 0$ leading to local flame broadening. We seek to understand such crucial reversal in the sign of the normal gradient of the flame speed, which is central to flame thickening and associated reduction in $\widetilde{S_{d,0}}$.

Conditionally averaged flame structures along their local normal directions from surface locations $c = c_0$ where $\kappa = 0$, are analyzed. Figure 8 shows the mean local flame structure (black for c and red for S_d/S_L) conditioned on $\kappa = 0$ for the flame surfaces $c_0 = 0.05, 0.2, 0.4$ and 0.6 for all the cases. The corresponding flame structures from standard laminar flame are shown in faint curves. The vertical grey line, i.e., $\xi/\delta_L = 0$ is the origin lying on the corresponding c_0 where $\kappa = 0$. Care is taken while generating the structures since S_d is undefined at $c = 0$ where $|\nabla c| = 0$ by Eq.1. Hence a point ($\kappa = 0$) is excluded if $c < 0.01$ in $-1 \le \xi/\delta_L \le 1$ along n. However, $\partial S_d/\partial n$ is indeed positive at the points on the flame surface conditioned on $\kappa = 0$ ($\xi/\delta_L = 0$) in agreement with Fig. 6. This is because such points are preceded by a sharp increase in S_d along n, starkly contrasting with any laminar flame structure. The V-shaped temperature profile just preceding the point of interest is also apparent. Figure 8 presents a second set of conditionally averaged local flame structures (from $c = c_0$ and $\kappa = 0$) along n which includes non-dimensional total curvature, $\kappa\delta_L$ in black, minimum and maximum non-dimensional principal curvatures, $\kappa_1\delta_L$ and $\kappa_2\delta_L$ in red and blue respectively. Coinciding with the peak in S_d and the valley in the c profiles, we observe a sharp drop in average $\kappa\delta_L$ and $\kappa_1\delta_L$ profiles just preceding $\xi/\delta_L = 0$ - the quintessential signature of cylindrical flame-flame interaction shown in Fig. 2. This implies that due to their ubiquity at large *Ka*, localized, cylindrical flame-flame interaction precedes the nearly flat locations of the flame surface in the direction of reactants, on average.

In summary, DNS results show that lean hydrogen-air turbulent flames at $\kappa = 0$ exhibit an enhancement in $\widetilde{S_d}$ due to tan-

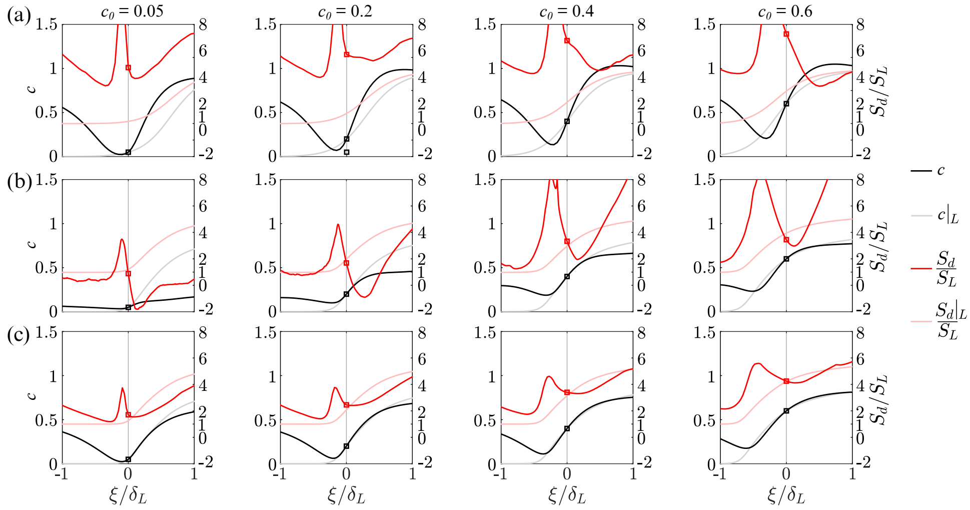

Figure 7. Mean local flame structures of c and S_d/S_L conditioned on $\kappa = 0$ at $c = c_0$ for (a) Le05Ka100 (b) Le08Ka1000 (c) Le1Ka100. The faint lines in the background show the corresponding standard laminar flame profiles.

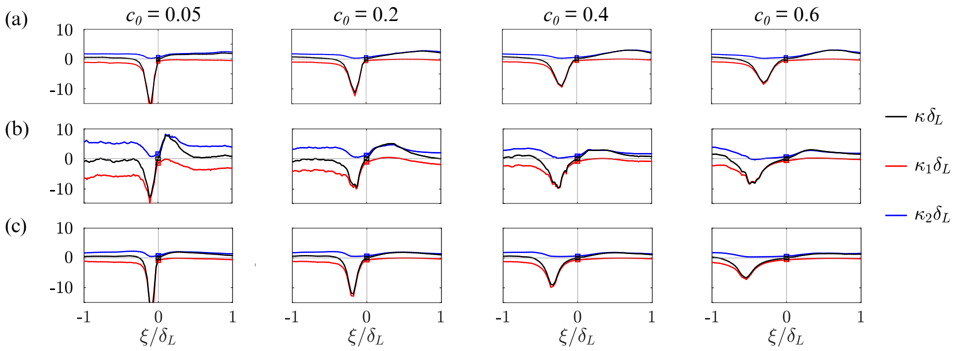

Figure 8. Mean local flame structures of $\kappa\delta_L$, $\kappa_1\delta_L$ and $\kappa_2\delta_L$ conditioned on $\kappa = 0$ for (a) Le05Ka100 (b) Le08Ka1000 (c) Le1Ka100.

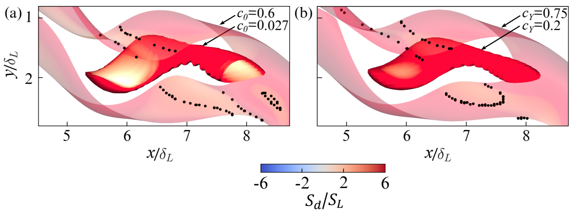

Figure 9. Segments of the iso-scalar surfaces of Le05Ka100 colored by S_d/S_L based on (a) T: $c_0 = 0.027$ and 0.6 (b) Y_{H_2}: $c_Y = 0.2$ and 0.75. The black markers denote the points with $\kappa = 0$ on (a) $c_0 = 0.6$ and (b) $c_Y = 0.75$.

gential straining by turbulence combined with the sub-unity Le. However, a decreased local temperature gradient attenuates this effect compared to the strained laminar flame counterpart. The local flame thickening of these turbulent flame segments are found to be mainly due to the neighboring flame-flame interaction. We visualize such a phenomenon in Fig. 9 using both isotherms and iso-Y_{H_2} surfaces in a) and b), respectively. The black markers denote the $\kappa = 0$ points on $c_0 = 0.6$ and $c_Y = 0.75$ iso-surfaces. From the viewpoint of an observer in these nearly flat yet strained locations, the flame-flame interaction at the neighboring, highly curved, near cylindrical surfaces increases S_d at those corresponding neighboring surfaces. This causes those neighboring surfaces to separate faster from the reference, resulting in flame thickening characterized by diminished scalar gradients. Hence, it is concluded that the flame-flame interaction plays an important role in characterizing turbulent flame propagation for flame segments at large curvatures as well as at highly strained, nearly flat regions.

Conclusions

Most parts of ultra-lean, large Ka hydrogen flames propagate faster in turbulence when compared to their standard laminar counterpart due to preferential diffusion effects. However, quantifying and explaining such enhancement using strained laminar flames has remained challenging. Mapping flame displacement speed (ratios) with the local structure represented by the thermal gradient (ratios), the reason for this difference systematically emerges. All investigated turbulent flames, irrespective of Le and Ka thicken on average when compared to the strained laminar flames at the same mean tangential strain-rate conditions. Such thickening is primarily due to reversed local flame speed gradients for all the large Ka flames investigated. The reversal occurs due to non-local but ubiquitous flame-flame interaction at large negative curvatures, which is shown to rapidly increase local flame displacement speed in the interacting regions, causing broadening within the flame structure. This work thus shows that strained laminar flame can be used to understand the limiting condition of local flame speed and structure in turbulence while their actual deviation has to be estimated, accounting for non-local flame-flame interaction modifying local flame speed gradients.

REFERENCES

Brandenburg, A., Collaboration, Pencil Code *et al.* 2018 `http://pencil-code.nordita.org/`, accessed: 2022-04-26.

Brouzet, D., Haghiri, A., Talei, M. & Brear, M. J. 2019 Annihilation events topology and their generated sound in turbulent premixed flames. *Combustion and Flame* **204**, 268–

277.

Chakraborty, N. & Cant, R., S. 2005 Influence of lewis number on curvature effects in turbulent premixed flame propagation in the thin reaction zones regime. *Physics of Fluids* **17** (10).

Chakraborty, N & Swaminathan, N 2007 Influence of the damköhler number on turbulence-scalar interaction in premixed flames. i. physical insight. *Phys. Fluids* **19** (4).

Chaudhuri, S. 2015 Life of flame particles embedded in premixed flames interacting with near isotropic turbulence. *Proceedings of the Combustion Institute* **35** (2), 1305–1312.

Chaudhuri, S., Akkerman, V. & Law, C. K. 2011 Spectral formulation of turbulent flame speed with consideration of hydrodynamic instability. *Physical Review E* **84**, 026322.

Chaudhuri, S., Kolla, H., Dave, H., L., Hawkes, E. R., Chen, J., H. & Law, C. K. 2017 Flame thickness and conditional scalar dissipation rate in a premixed temporal turbulent reacting jet. *Combustion and Flame* **184**, 273–285.

Chaudhuri, S. & Savard, B. 2023 Turbulent flame speed based on the mass flow rate: Theory and dns. *Combustion and Flame* **252**, 112735.

Chomiak, J. & Lipatnikov, A. N 2023 Simple criterion of importance of laminar flame instabilities in premixed turbulent combustion of mixtures characterized by low lewis numbers. *Physical Review E* **107** (1), 015102.

Chu, H., Berger, L., Grenga, T., Wu, Z. & Pitsch, H. 2023 Effects of differential diffusion on hydrogen flame kernel development under engine conditions. *Proceedings of the Combustion Institute* **39** (2), 2129–2138.

Coulon, V., Gaucherand, J., Xing, V., Laera, D., Lapeyre, C. & Poinsot, T. 2023 Direct numerical simulations of methane, ammonia-hydrogen and hydrogen turbulent premixed flames. *Combustion and Flame* **256**, 112933.

Dave, H. L. & Chaudhuri, S. 2020 Evolution of local flame displacement speeds in turbulence. *Journal of Fluid Mechanics* **884**, A46.

Dave, H. L., Mohan, A. & Chaudhuri, S. 2018 Genesis and evolution of premixed flames in turbulence. *Combustion and Flame* **196**, 386–399.

Detomaso, N., Hok, J., J., Dounia, O., Laera, D. & Poinsot, T. 2023 A generalization of the thickened flame model for stretched flames. *Combustion and Flame* **258**, 113080.

Dopazo, C., Cifuentes, L., Martin, J. & Jimenez, C. 2015 Strain rates normal to approaching iso-scalar surfaces in a turbulent premixed flame. *Combustion and Flame* **162** (5), 1729–1736.

Echekki, T. & Chen, J. H. 1996 Unsteady strain rate and curvature effects in turbulent premixed methane-air flames. *Combustion and Flame* **106**, 184–190.

Gkantonas, S.and Talibi, M., Balachandran, R. & Mastorakos, E. 2023 Hydrogen combustion in gas turbines. *Hydrogen for Future Thermal Engines* pp. 407–428.

Griffiths, R. A. C., Chen, J. H., Kolla, H., Cant, R. S. & Kollmann, W. 2015 Three-dimensional topology of turbulent premixed flame interaction. *Proceedings of the Combustion Institute* **35** (2), 1341–1348.

Howarth, T., L., Hunt, E., F. & Aspden, A., J. 2023 Thermodiffusively-unstable lean premixed hydrogen flames: Phenomenology, empirical modelling, and thermal leading points. *Combustion and Flame* **253**, 112811.

Howarth, T. L. & Aspden, A. J. 2022 An empirical characteristic scaling model for freely-propagating lean premixed hydrogen flames. *Combustion and Flame* **237**, 111805.

Im, H., G., Bechtold, J., K. & Law, C., K. 1996 Response of counterflow premixed flames to oscillating strain rates. *Combustion and Flame* **105** (3), 358–372.

Law, C. K. 2006 *Combustion Physics*. Cambridge University Press.

Lee, H., C., Dai, P., Wan, M. & Lipatnikov, A., N. 2022 A dns study of extreme and leading points in lean hydrogen-air turbulent flames - part ii: Local velocity field and flame topology. *Combust and Flame* **235**, 111712.

Lee, H. C., Dai, P., Wan, M & Lipatnikov, A., N. 2023 Displacement speed, flame surface density and burning rate in highly turbulent premixed flames characterized by low lewis numbers. *Journal of Fluid Mechanics* **961**, A21.

Li, J., Zhao, Z., Kazakov, A. & Dryer, F. 2004 An updated comprehensive kinetic model of hydrogen combustion. *International Journal of Chemical Kinetics* **36**, 566 – 575.

Matalon, M., Cui, C. & Bechtold, J. K. 2003 Hydrodynamic theory of premixed flames: effects of stoichiometry, variable transport coefficients and arbitrary reaction orders. *J. Fluid Mech.* **487**, 179–210.

Peters, N 2000 *Turbulent Combustion*. Cambridge University Press.

Peters, N., Terhoeven, P., Chen, J., H & Echekki, T. 1998 Statistics of flame displacement speeds from computations of 2-d unsteady methane-air flames. *Symposium (International) on Combustion* **27** (1), 833–839.

Pope, S., B., Yeung, P., K. & Girimaji, S., S. 1989 The curvature of material surfaces in isotropic turbulence. *Physics of Fluids A: Fluid Dynamics* **1** (12), 2010–2018.

Rieth, M., Gruber, A. & Chen, J., H. 2023 The effect of pressure on lean premixed hydrogen-air flames. *Combustion and Flame* **250**, 112514.

Rieth, M., Gruber, A., Williams, F. A. & Chen, J., H. 2022 Enhanced burning rates in hydrogen-enriched turbulent premixed flames by diffusion of molecular and atomic hydrogen. *Combustion and Flame* **239**, 111740.

Song, W., Hernández-Pérez, F., E. & Im, H., G. 2022 Diffusive effects of hydrogen on pressurized lean turbulent hydrogen-air premixed flames. *Combustion and Flame* **246**, 112423.

Song, W., Hernandez-Perez, F. E., Tingas, E. A. & Im, H. G. 2021 Statistics of local and global flame speeds for turbulent H2/air premixed flames at high Karlovitz numbers. *Combust ion and Flame* **232**, 111523.

Trivedi, S., Griffiths, R., Kolla, H., Chen, J. H. & Cant, R. S. 2019 Topology of pocket formation in turbulent premixed flames. *Proceedings of the Combustion Institute* **37** (2), 2619–2626.

Vance, Faizan H, Shoshin, Y, De Goey, LPH & van Oijen, Jeroen A 2021 A physical relationship between consumption and displacement speed for premixed flames with finite thickness. *Proc. Combust. Inst.* **38** (2), 2215–2223.

Wang, H., Hawkes, E. R., Chen, J., H., Zhou, B., Li, Z. & Aldén, M. 2017 Direct numerical simulations of a high karlovitz number laboratory premixed jet flame – an analysis of flame stretch and flame thickening. *Journal of Fluid Mechanics* **815**, 511–536.

Yuvraj, Ardebili, Y., N., Song, W., Im, H. G., Law, C. K. & Chaudhuri, S. 2023 On flame speed enhancement in turbulent premixed hydrogen-air flames during local flame-flame interaction. *Combustion and Flame* **257**, 113017.

Yuvraj, Song, W., Dave, H., L., Im, H., G. & Chaudhuri, S. 2022 Local flame displacement speeds of hydrogen-air premixed flames in moderate to intense turbulence. *Combustion and Flame* **236**, 111812.

Zeldovich, Y. B. 2014 *Selected Works of Yakov Borisovich Zeldovich, Volume I: Chemical Physics and Hydrodynamics*, , vol. 140. Princeton University Press.